NASA'S REMOTELY SENSED PRECIPITATION

A Reservoir for Applications Users

Dalia B. Kirschbaum, George J. Huffman, Robert F. Adler, Scott Braun, Kevin Garrett, Erin Jones, Amy McNally, Gail Skofronick-Jackson, Erich Stocker, Huan Wu, and Benjamin F. Zaitchik

NASA's precipitation measurement missions provide critical precipitation information to end users that improves understanding of Earth's water cycle and enhances decision-making at local to global scales.

Precipitation is the fundamental source of freshwater in the water cycle. If one could collect all of the water in the atmosphere, including water vapor, clouds, and precipitation, it would account for 4% of the total freshwater and 0.01% of the total water on Earth (USGS 2016). Despite its small fraction of the total, precipitation is the critical pipeline that replenishes aquifers, sustains agriculture, and enables our economy to grow (Shepherd et al. 2016). Where and when precipitation is falling has historically been recorded by surface rain gauges. However, if one takes the total surface area of the orifices for all the rain gauges routinely used in the generation of global precipitation products and puts them together, they would only cover the area of two basketball courts (Kidd et al. 2017). As the fleet of remote sensing platforms to measure precipitation has grown, increasingly rapid and easy access to precipitation datasets has expanded data use, providing a growing legacy of high-quality precipitation data that has enabled new science and new applications to benefit society (Kucera et al. 2013).

In 2016, the National Aeronautics and Space Administration (NASA) had over two dozen satellites and instruments in orbit around Earth that are continually taking the pulse of our planet. NASA supports and enables a diverse range of applications of Earth science data. In this context, "applications" refers to the use of satellite and airborne data and related products in decision-making for societal benefit (Brown and Escobar 2014). The ultimate goals of these efforts are to effectively and efficiently identify,

AFFILIATIONS: Kirschbaum, Huffman, Braun, Skofronick-Jackson, and Stocker—NASA Goddard Space Flight Center, Greenbelt, Maryland; Adler and Wu—Earth System Science Interdisciplinary Center, University of Maryland, College Park, College Park, Maryland; Garrett and Jones—Riverside Technology, Inc., and NOAA/NESDIS/Center for Satellite Applications and Research, College Park, Maryland; McNally—NASA Goddard Space Flight Center, Greenbelt, and Earth System Science Interdisciplinary Center, University of Maryland, College Park, College Park, Maryland; Zaitchik—The Johns Hopkins University, Baltimore, Maryland
CORRESPONDING AUTHOR: Dalia Kirschbaum, dalia.b.kirschbaum@nasa.gov

The abstract for this article can be found in this issue, following the table of contents.
DOI:10.1175/BAMS-D-15-00296.1

In final form 13 September 2016

respond to, and address the needs of current and potential user groups by guiding how the application of satellite data, models, and products can be converted into actionable and user-friendly information to support policy- and decision-making.

NASA's Precipitation Measurement Missions (PMM) have established a long history of advanced precipitation measurements from space. The Tropical Rainfall Measuring Mission (TRMM), co-led by NASA and the Japan Aerospace Exploration Agency (JAXA), was launched in 1997 and provided unprecedented data on heavy to moderate rainfall in Earth's tropics and subtropics for over 17 years (Simpson et al. 1996; Kummerow et al. 1998). The TRMM spacecraft exhausted its fuel and subsequently reentered Earth's atmosphere in June 2015. The Global Precipitation Measurement (GPM) *Core Observatory*, also a joint mission by NASA and JAXA, was launched in February 2014. The GPM mission continues and expands TRMM's legacy by estimating precipitation ranging from light rain to heavy rain (0.2–110 mm h^{-1}) and snow over the latitude band 65°N–65°S. The GPM *Core Observatory* is designed to work with and anchor a constellation of satellites and ground systems from partner agencies located in the United States, Japan, Europe, and India (Hou et al. 2014; Fig. 1).

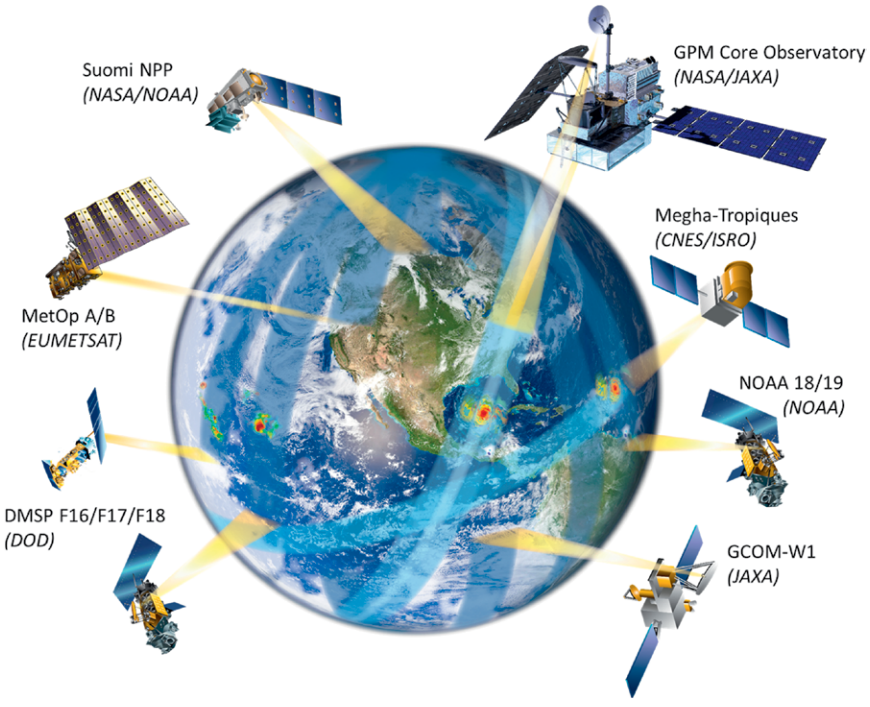

Fig. 1. The GPM constellation uses data from several microwave imagers and sounders, contributed by partner agencies and countries. As of May 2016, these include the U.S. Defense Meteorological Satellite Program (DMSP) series, JAXA Global Change Observation Mission–Water 1 (GCOM-W1), the NASA-JAXA GPM *Core Observatory*, the Centre National d'Etudies Spatiales (CNES) of France and the Indian Space Research Organization (ISRO) Megha-Tropiques, the European Organisation for the Exploitation of Meteorological Satellites (EUMETSAT) Meteorological Operational (MetOp) series, the NOAA series, and the NASA–NOAA *Suomi-National Polar-Orbiting Partnership (SNPP)* (modified from Hou et al. 2014).

One way that NASA determines the success and relevance of its missions is by understanding and quantifying how the data are applied within different communities of end users, including national weather and hydrology agencies, national and international nongovernment organizations (NGOs), and private companies. During TRMM, a range of diverse applications of precipitation information was developed across societal benefit areas. The new generation of GPM precipitation products seeks to advance the societal applications of the data to better address the needs of the end users and their applications areas (Table 1). In this paper, we outline the current and planned PMM activities, specifically focusing on the GPM suite of data products relevant for an applications-focused audience. We then provide case studies of how TRMM and GPM data have been applied across four thematic areas: tropical cyclone track forecasting, flood modeling, agricultural monitoring, and disease tracking.

NASA'S PMM: BUILDING A LEGACY. TRMM was a research satellite designed to improve our understanding of the distribution and variability of precipitation at daily to yearly time scales over the tropical and subtropical regions of the Earth. It provided much-needed information on rainfall and its associated latent heat release that helps to power global atmospheric circulation and influence both weather and climate. The TRMM satellite had two primary precipitation-sensing instruments:

Table 1. Examples of applications' thematic areas and topics where satellite precipitation estimates are being used for situational awareness and decision-making. More information and specific case studies can be found in Ward and Kirschbaum (2014) and Ward et al. (2015).

Area	Topic	Application
Extreme events and disasters	Flooding	Incorporation in hydrologic and routing models for flood estimation, streamflow, and inundation
	Landslides	Nowcasting of potential landslide activity, rainfall intensity, and duration characteristics for landslide occurrence
	Tropical cyclones	Improved characterization of tropical cyclone track, intensity, and 3D visualization
	Reinsurance	Definition of extreme precipitation thresholds to support microinsurance
	Wildfires	Management and situational awareness of rainfall accumulation in affected areas
	Disaster response	Situational awareness of extreme precipitation in potentially affected areas
Water resources and agriculture	Drought	Evaluation of precipitation anomalies leveraging extended temporal record
	Water resource management	Assessment of freshwater inputs to basins and reservoirs to quantify water fluxes
	Famine early warning	Inclusion of satellite precipitation in crop forecast modeling
	Food security	Assessing water crises that may impact water balance in vulnerable areas
Weather and climate modeling	Numerical weather prediction	Assimilation of Level 1 brightness temperatures within NWP modeling for initializing model runs
	Land surface modeling	Data assimilation into land surface models to estimate environmental variables
	Climate variability and change	Verification and validation of climate modeling precipitation outputs
Public health and ecology	Disease tracking	Tracking precipitation anomalies with environmental conditions for vector or waterborne diseases
	Animal migration	Monitor changes in precipitation that are associated with animal migration patterns

the TRMM Microwave Imager (TMI) was a conically scanning nine-channel passive microwave radiometer with a swath width of 880 km, and the Precipitation Radar (PR) was a 13.8-GHz-frequency radar with a swath width of 250 km (Kummerow et al. 1998).

A NASA-based algorithm called the TRMM Multisatellite Precipitation Analysis (TMPA) merged precipitation analyses from TMI, radiometers flying on other satellites (both conically and cross-track scanning), geosynchronous infrared (IR) sensors, and precipitation gauges to create a product with a spatial resolution of 0.25° × 0.25° over the latitude band 50°N–50°S (Huffman et al. 2007, 2010). The dataset currently contains two sets of products. The first is a 3-hourly combined microwave–IR precipitation estimate provided in two forms: a near-real-time product (8-h latency, product 3B42 RT) starting in February 2000 that is adjusted using a gauge climatology and a research-quality, 3-hourly combined microwave–infrared (IR) precipitation estimate with month-to-month coincident gauge adjustment (2-month latency, product 3B42) starting in January 1998. A monthly combined microwave–IR gauge product (3B43) is also provided, starting in January 1998. Despite the end of TRMM satellite operations, the TMPA algorithm will continue to be produced through 2018 using the other radiometers in the constellation in order to provide overlap for applications users to test and transition their models and applications from TRMM to GPM products. Figure 2 displays the 16-yr annual rainfall average

from the TRMM 3B43 product, showing the dominant pattern of the intertropical convergence zone (ITCZ) in the equatorial Pacific. Table 2 summarizes selected TRMM and GPM products, their resolutions, and latencies.

The GPM core satellite carries two instruments that provide increased sensitivity to light rain rates and snowfall, as well as new information on particle drop size distribution, relative to TRMM. The GPM Microwave Imager (GMI) is a radiometer with 13 channels measuring microwave energy at frequencies ranging from 10 to 183 GHz that covers a swath of 885 km (550 miles). The Dual-Frequency Precipitation Radar (DPR) has both a KaPR (operating at 35.5 GHz) and a KuPR (13.6 GHz) with swaths of 125 and 245 km, respectively (Hou et al. 2014). Together, these instruments provide new insights into the behavior and characteristics of precipitation and provide a vital source for calibrating retrievals from other precipitation sensors.

The Integrated Multisatellite Retrievals for GPM (IMERG) is NASA's multisatellite algorithm that intercalibrates, merges, and time-interpolates "all" satellite microwave precipitation estimates in the GPM constellation, then incorporates microwave-calibrated IR satellite estimates and precipitation gauge analyses (Huffman et al. 2015). IMERG uses the GPM Combined Instrument precipitation estimate to intercalibrate all available microwave data, similar to the TMPA approach, but introduces the microwave time-interpolation scheme provided in the Climate Prediction Center (CPC) morphing–Kalman filter technique (KF-CMORPH; Joyce and Xie 2011), which follows the estimated motion of the precipitation systems. The IR precipitation estimates are computed with the Precipitation Estimation from Remotely Sensed Information Using Artificial Neural Networks–Cloud Classification System (PERSIANN-CCS; Hong et al. 2004). The result is a map of precipitation rate (mm h^{-1}) every 30 min at a 0.1° × 0.1° resolution, currently covering the latitude band 60°N–60°S, with expansion to all latitudes in the future.

IMERG has products with various latencies (Table 2), starting with a rapid precipitation estimate and successively providing improved estimates as more data become available. The "Early" IMERG product is IMERG product is available 4–5 h after observation time after observation time and is geared toward end users that require immediate precipitation data such as disaster response. The "Late" product is available 14–15 h after observation time and is used by the agricultural modeling and public health communities, among others. The "Final" product uses monthly gauge data to create a research-level satellite–gauge product that is available ~3 months after the observation month.

Data availability and access. Data from the GPM and TRMM missions are made freely available to the public in a variety of formats and through several different archives at NASA, outlined at http://pmm.nasa.gov/data-access/. The Precipitation Processing System (PPS), housed at NASA's Goddard Space Flight Center, processes, analyzes, and archives data from the TRMM and GPM missions and partner satellites. Automatic, free, and immediate online registration (http://registration.pps.eosdis.nasa.gov/registration) is required to gain access to the PPS TRMM/GPM FTP data archives. In addition to the original 30-min IMERG products, there are IMERG accumulation products at 3 h and 1, 3, and 7 days produced as TIFF format with a world file. Data are searchable and exportable through PPS's STORM system (https://storm.pps.eosdis.nasa.gov/storm/). A variety of visualization and analysis tools are also available through the Goddard Earth Sciences Data and Information Services Center (GES DISC; http://daac.gsfc.nasa.gov/) and through the PMM website (http://pmm.nasa.gov). Information on data available and formats are provided at http://pmm.nasa.gov/data-access/downloads. Within each portal, website, and visualization interface, there is a strong emphasis on user support from the NASA community. These systems are continually evolving and advancing

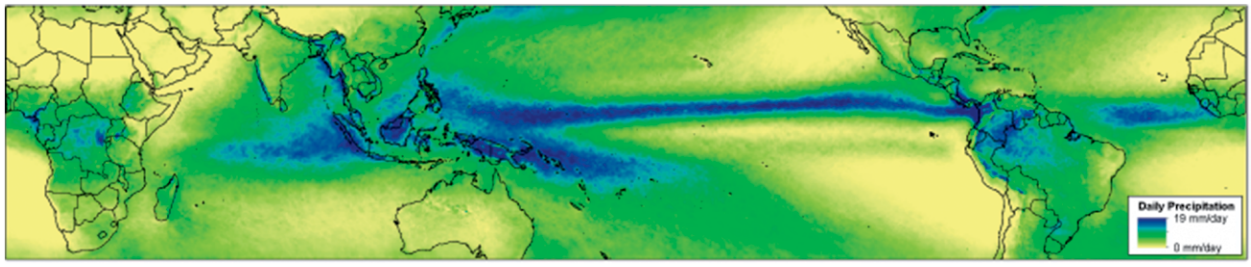

Fig. 2. TRMM annual average rainfall (mm day^{-1}) from 1998 to 2013.

their capabilities, fueled by feedback from the user communities.

Using precipitation data to serve society. NASA's emphasis in applied sciences is focused on engaging people and organizations in the applications community for early and ongoing involvement in satellite and instrument mission planning, operation, and resulting products. The goal is to enhance the value and return on investment from NASA satellite missions by enabling users to anticipate potential applications of upcoming data, provide feedback on data products, and be prepared to use the data soon after launch. Through the nearly two decades of TRMM and GPM precipitation data, a broad range of users and applications has been established that demonstrates the applicability and relevance of these precipitation measurements across agencies, research institutions, and the global community.

APPLICATIONS CASE STUDIES. This paper showcases four examples of how TRMM and now GPM data are being applied within different data assimilation and modeling scenarios and for diverse end-user audiences. These case studies demonstrate how the availability and continuity of satellite-based precipitation data records can influence and enhance scientific research and societal issues in ways that are not otherwise possible.

GMI impact study for hurricane track prediction. Numerical weather prediction centers around the

Table 2. Selected product descriptions for TRMM and GPM. The full list is available under the TRMM and GPM hot links at https://pmm.nasa.gov/data-access/. TRMM and GPM products are available in near-real-time (NRT) and/or production versions.

Level	Algorithm name	Description	Resolution		Coverage	Latency
			Space	Time		
GPM Level 1	1B-GMI	GMI brightness temperatures	Varies by channel	16 orbits per day	Latitudes 70°N–70°S, past week (NRT)	1 h (NRT); 6 h (production)
	1C-GMI	Calibrated GMI brightness temperatures	Varies by channel	16 orbits per day	Latitudes 70°N–70°S, past week (NRT)	1 h (NRT); 6 h (production)
GPM Level 2	2A-DPR	DPR Ka and Ku single-orbit rainfall estimates	5 km × 5 km (at nadir), 125-m vertical resolution	16 orbits per day	Latitudes 67°N–67°S, Mar 2014–present	20–120 min (NRT); 24 h (production)
	2A-GPROF-GMI	GMI single-orbit rainfall estimates	11 km × 18 km	16 orbits per day	Orbital, 70°N–70°S	1 h (NRT); 40 h (production)
	2B-CMB	Combined GMI + DPR single-orbit rainfall estimates	5 km × 5 km (at nadir), 250-m vertical resolution	16 orbits per day	Orbital, 67°N–67°S	3 h (NRT); 40 h (production)
GPM Level 3	IMERG	Integrated Multisatellite Retrievals for GPM	0.1° × 0.1°	30 min	Gridded, 60°N–60°S	4–5 h (NRT/Early run) 14–15 h (NRT/Late run) 3 months (production/Final run)
	3-CMB	Combined GMI + DPR rainfall averages	0.25°, 5°	Daily, monthly	Gridded, 70°N–70°S	Daily, monthly (production only)
TRMM Level 3	TMPA 3B42	TRMM Multisatellite Precipitation Analysis	0.25° × 0.25°	3-hourly	Gridded, 50°N–50°S	8 h 2 months
	TMPA 3B43		0.25°, 5°	Monthly		2 months from last date in month

world rely on microwave and IR-based observations to improve weather prediction and forecasting of tropical cyclone track and intensity. This case study evaluates the impact of assimilating GMI into a track prediction for Tropical Storm Julio, which formed in the east Pacific basin on 4 August 2014, approximately 680 nautical miles south-southwest of Baja California Sur, Mexico (Stewart and Jacobson 2016). Initial forecasts of Julio showed the storm intensifying into a powerful hurricane, with possible impacts on the Hawaiian Islands following directly in the wake of Tropical Storm Iselle, which made landfall on the Big Island near Pahala on 8 August. Fortunately, Julio shifted northward of Hawaii, resulting in no major impacts or damage. Here we present simulations performed to assess the potential impact of using GMI data in numerical weather prediction (NWP) models. The reduction of forecast track uncertainty in this case, if applicable more generally, can provide improved lead time to aid in disaster preparedness.

Partners in the U.S. Joint Center for Satellite Data Assimilation (JCSDA), including the NOAA/NESDIS/Center for Satellite Applications and Research (STAR) and the NASA Global Modeling and Assimilation Office (GMAO), tested processing and assimilating GMI passive microwave observations as input for the global data assimilation systems used to initialize NWP forecast models. In STAR, the effort focused on the assimilation of clear-sky, ocean-only brightness temperatures from the GMI Level 1C-R product (NASA 2015) toward improvement of the analysis and forecast skill in the NOAA Global Data Assimilation System/Global Forecast System (GDAS/GFS; Wang et al. 2013). The Level 1C-R data co-registers the low- and high-frequency observations, allowing for the synergistic use of all GMI channels to maximize the information content contained in the observations during the assimilation.

To assess the impact of assimilating GMI observations on the forecast track of Julio, two experiments were run in the GDAS/GFS covering the first two weeks of August 2014. The first experiment (CTRL) included all conventional and satellite observations operationally assimilated in the GDAS/GFS. The second experiment (DAGMI) added GMI observations on top of the configuration of the CTRL experiment. Both forecast experiments were run at T670/L64 (~25 km) resolution, and only the GFS forecasts initialized at 0000 UTC between 4 and 12 August were assessed. Figure 3 shows the track forecast for the CTRL experiment (Fig. 3a) and DAGMI experiment (Fig. 3b) for each GFS forecast. Each point represents a forecast storm location at 24-h intervals, beginning with the analysis time and ending at the forecast time valid for the last reported official "best" track location (0000 UTC 14 August, black line with hurricane symbols). Early in the period, each experiment showed similar tracks trending northward with each forecast cycle, potentially impacting Hawaii around Day 6 from the 0000 UTC 5 August forecast. However, for the 6 August forecast and beyond, DAGMI shows less uncertainty, more consistency cycle to cycle, and better agreement with the official track that there would be no direct impact from Julio on Hawaii. For the CTRL experiment, the 6 August forecast keeps Julio closer

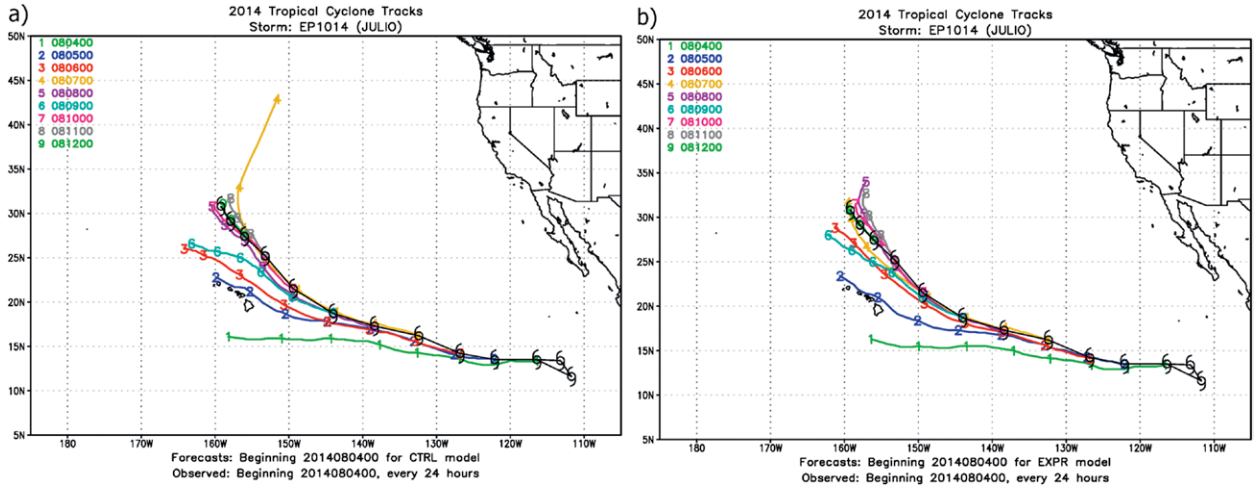

Fig. 3. Julio track forecasts initialized at 0000 UTC between 4 and 12 Aug 2014 for the (a) CNTL and (b) DAGMI experiments. The official "best" track is shown by the black line with hurricane symbols. Each point represents the forecast location at 24-h intervals starting with the analysis time and ending with the forecast hour valid at the last best-track data point.

to Hawaii relative to DAGMI, while the 9 August forecast moves the track back toward Hawaii relative to the previous two forecast cycles. This track shift back toward Hawaii on 9 August is particularly important as it gives rise to potential impacts with only 2 days of lead time. Note also that the CTRL forecast for 7 August shows the storm rapidly accelerating into the midlatitudes.

Forecast uncertainty of an upper-level ridge north of Hawaii was the primary factor in the forecast track uncertainty of Julio (Stewart 2014). Figure 4a illustrates the ridge in place depicted by the 500-hPa geopotential height analysis valid at 0000 UTC 6 August, along with the 700-hPa flow represented by the streamlines. The low geopotential heights near 17°N, 141°W are associated with Hurricane Iselle, which was steered toward Hawaii as the ridge held in place. Forecast models at the time, as well as with the CTRL experiment, were inconsistent on the erosion of the ridge that would ultimately allow Julio to track north of Hawaii. Figure 4b shows the 500-hPa geopotential height analysis, along with the 5-day forecast of 500-hPa geopotential height for the CTRL and DAGMI experiments, valid at 0000 UTC 11 August. It is evident that the DAGMI forecast with assimilated GMI data shows greater erosion of the upper-level ridge than the CTRL forecast, and the subsequent shift in the Julio forecast track farther north of Hawaii, closer to the analysis position.

Although there is positive impact from the assimilation of GMI observations on the track forecast of Julio in the NOAA GDAS/GFS, cases from many hurricane seasons and basins are required to establish the statistical significance of enhancing the NWP data assimilation systems. Not only do GMI's high-quality radiometer observations add to the robustness of the global satellite observing system, but they also add unique observations that accurately characterize hydrological parameters important for the moist physics schemes that help drive NWP. Greater impact in NWP is expected in the future from GMI as data assimilation systems become more effective at assimilating radiometric observations affected by clouds and precipitation.

Global flood monitoring. Access to near-real-time precipitation estimates on a global scale is valuable for regional assessments of current or potential flood events. The TMPA precipitation estimates are input to a Global Flood Monitoring System (GFMS; http://flood.umd.edu/) with the goal of providing near-real-time flood estimates and forecasts between 50°N and 50°S (Wu et al. 2014). This system is also in the process of testing IMERG precipitation estimates.

GFMS couples the Variable Infiltration Capacity (VIC) land surface model (Liang et al. 1994) and the Dominant River Tracing Routing (DRTR) model to form the Dominant River routing Integrated with VIC Environment (DRIVE) modeling system. To establish percentile thresholds for flood detection within the GFMS system, the DRIVE model was run retrospectively for 15 years using the TMPA record to provide a history of water depth and streamflow at 3-hourly, 0.125° resolution. The 95th percentile

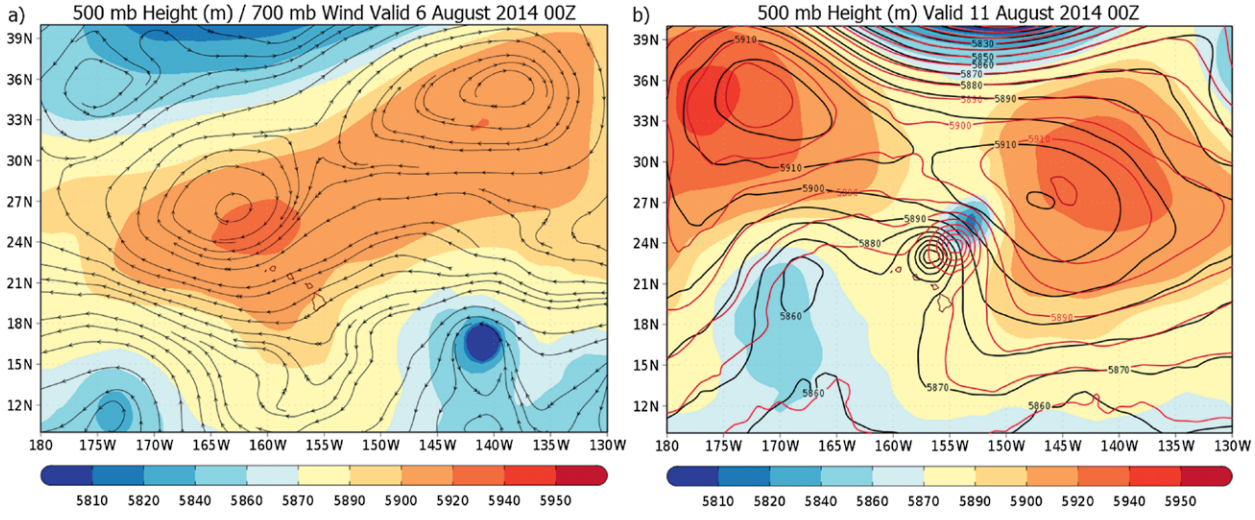

Fig. 4. (a) The 500-hPa geopotential height analysis (m, shaded contours) and 700-hPa wind (streamlines) valid at 0000 UTC 6 Aug, and (b) the 500-hPa geopotential height analysis (shaded contours) valid at 0000 UTC 11 Aug and 5-day forecasts of 500-hPa geopotential height for the CTRL experiment (black contours) and DAGMI experiment (red contours) valid at 0000 UTC 11 Aug.

was selected to represent water depth conditions above which flooding is likely (Wu et al. 2012, 2014). GFMS identifies potential flood areas in real time and provides temporal histories of flooding conditions at each pixel, including estimates of flood detection/intensity (water depth above the threshold) and streamflow (and its flood threshold).

The resulting products are designed to provide users with situational awareness of potential flooding conditions and associated triggering variables. These variables include 1-, 3-, and 7-day TMPA precipitation totals and a global precipitation forecast from the Goddard Earth Observing System, version 5 (GEOS-5; Molod et al. 2015), that is used to extend the hydrological calculations out to 5 days. In addition to the global model run at 0.125° spatial resolution, finer-resolution (1 km) global streamflow, surface water storage, and inundation mapping estimates are computed using the DRTR routing scheme and are available in real time. The 1-km results are a key step toward providing estimated high-resolution flood inundation maps that would complement satellite-based inundation estimates, for example, from the Moderate Resolution Imaging Spectroradiometer (MODIS).

The current modeling system also takes advantage of the higher spatial resolution and the more accurate instantaneous precipitation estimates from IMERG. Currently, IMERG data are aggregated to 3-h, 0.125° resolution to maintain consistency with the current GFMS using TMPA and to allow for a direct comparison of the real-time TMPA and IMERG products and consequent differences in flood calculations. Finer spatiotemporal resolutions at 0.1° and 0.0625° and 0.5-h intervals are being explored.

Figure 5 shows an example of how GFMS may be utilized for decision support. Very heavy rain (TMPA estimated over 1,100 mm) in mid- to late December 2014 in Malaysia produced significant floods that resulted in 17 fatalities and an estimated USD $284 million in damage (Guha-Sapir et al. 2014). Figure 5 illustrates the GFMS 0.125° product, showing streamflow above flood threshold (Fig. 5a) for affected locations on 27 December, and a time series for one of the affected rivers that shows both the previously

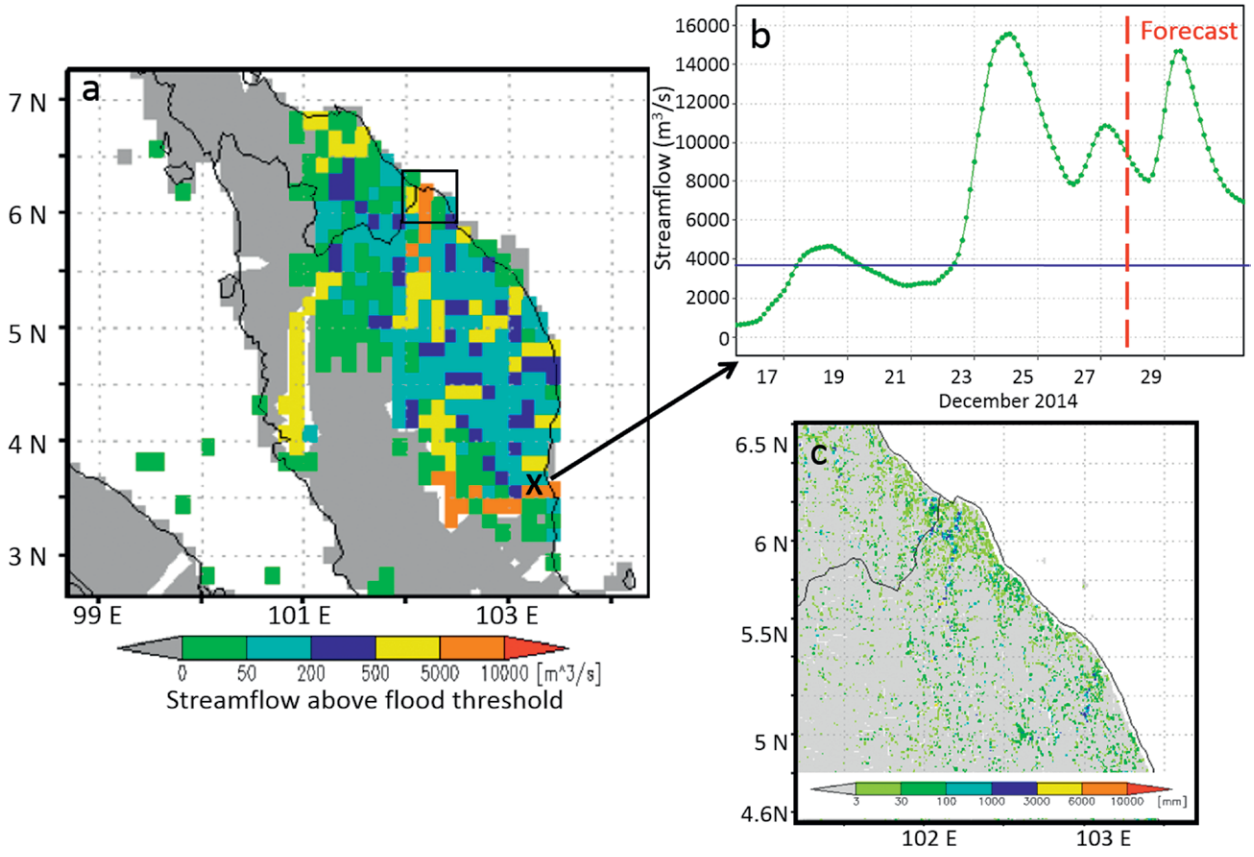

Fig. 5. Malaysia flooding in Dec 2014 as estimated from GFMS, showing (a) a map of streamflow above flood threshold on 27 Dec, (b) streamflow time history (green) at a point (indicated by the X) including the forecast (right side of red vertical line) from 27 to 31 Dec [note the streamflow flood threshold (blue) at the point in question], and (c) 1-km inundation estimate for inset black box shown in (a).

modeled estimates using TMPA and a forecast for the next few days using the GEOS-5 precipitation estimates (Fig. 5b). The GFMS can also be readily used to compare the intensity of the current event to previous events through the use of archived model calculations using the 1998 to present TMPA precipitation record. Figure 5c shows the experimental 1-km-resolution inundation estimate for the small box in Fig. 5a based on 1-km streamflow model results. We expect the finer time and space resolution of the GPM IMERG product to significantly enhance this kind of valuable information that will have important application benefits.

The GFMS has been an important input in catastrophe response activities by humanitarian relief agencies such as United Nations World Food Program (WFP) and the International Federation of Red Cross and Red Crescent Societies (Gray 2015). The WFP's Emergency Preparedness and Support Division in Rome monitors weather and the potential for flooding around the globe in order to support quick responses to inundated areas and affected communities. In developing countries with limited infrastructure, the WFP uses GFMS flood estimates, such as in Fig. 5, to anticipate flood events, help emergency responders assess potential risks, and help decision-makers prioritize aid efforts. The GFMS data have been integrated in WFP's developed tools on a daily basis.

Precipitation estimates for remote agricultural drought monitoring. Remotely sensed rainfall is a critical part of hydroclimate monitoring for organizations that track food and water security, like the Famine Early Warning Systems Network (FEWS NET; www.fews.net). In addition to the amount and distribution of rainfall throughout the season, the timing of the onset of rains or start of season (SOS) is an important parameter for early estimation of growing season outcomes like crop yield loss (Brown and de Beurs 2008). For example, SOS is a parameter in the Water Requirement Satisfaction Index (WRSI; Verdin and Klaver 2002) that has been used in conjunction with historic yield observations to develop drought vulnerability models that estimate crop yield loss in southern Africa and western Sahelian Africa (Jayanthi et al. 2014) and Ethiopia (Senay and Verdin 2003).

FEWS NET routinely estimates SOS with African Rainfall Estimation Algorithm, version 2 (RFE2), and Climate Hazards Group Infrared Precipitation with Station Data (CHIRPS). Figure 6 shows these two products with IMERG for comparison for SOS in southern Africa for the 2015/16 growing season. The operational rainfall product NOAA/CPC RFE2, and the IMERG-Late both have less than 1-day latency, which is important for answering questions at 1–30-day time scales. For comparison we show CHIRPS, a gauge-corrected product available at ~1 month latency, which is adequate for questions at the seasonal time scale. On a per pixel basis, SOS is determined using rainfall threshold criteria (AGRHYMET 1996). Each pixel is tested to identify the first dekad (~10-day period, 3 per month, 36 per year; WMO 1992) in which at least 25 mm of rain fell. To test for a "false start" that would result in failed plantings, the next two dekads' precipitation amounts are required to total at least 20 mm. If that criterion is not met, testing for the first SOS dekad resumes. The resulting maps (Fig. 6) show the dekad number of the SOS estimate for each grid cell.

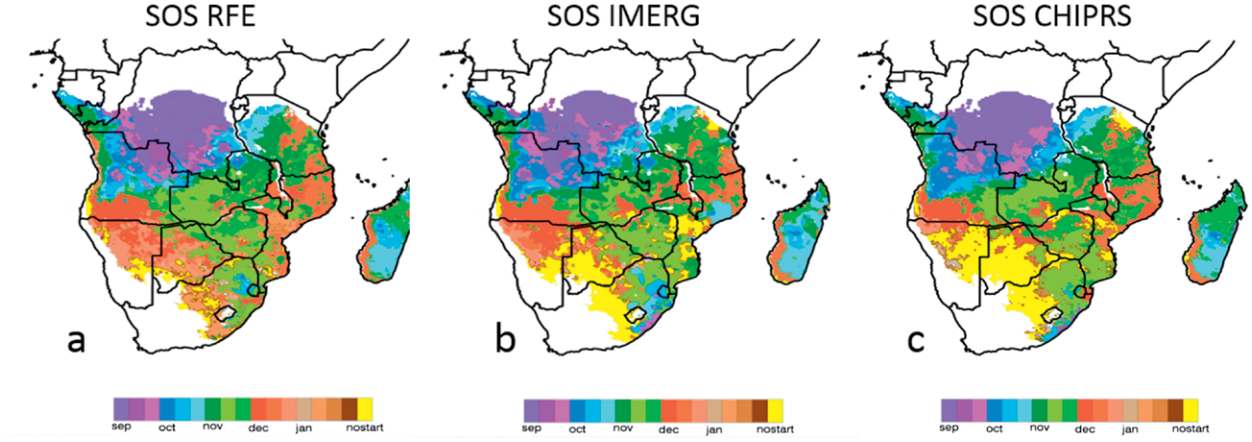

Fig. 6. SOS for the 2015/16 southern Africa growing season, computed with three different satellite-derived rainfall estimates: (a) RFE2 and (b) IMERG-Late are available in near–real time, while (c) CHIRPS is bias-corrected using rain gauge data with 1-month latency.

During the 2015/16 season, drought conditions affected many countries across Southern Africa because of a delayed start and erratic distribution of early season (October–December) rainfall (FEWS-NET 2016). The estimated onset of rains from IMERG agrees with the "no start" designation across parts of Southern Africa, Botswana, and Namibia, as well as central Mozambique. Meanwhile, RFE2 tends to show a February SOS where IMERG and CHIRPS show no start (southern Africa, central Mozambique). The lack of regularly reporting rainfall stations explains some of the differences between the three estimates. IMERG and RFE2 blend World Meteorological Organization (WMO) Global Telecommunication System (GTS) stations available in near–real time. With its longer latency, CHIRPS blends in stations from both the GTS and other sources (e.g., www.sasscal.org; Funk et al. 2015). To deal with uncertainty inherent in sparsely gauged, food-insecure regions, FEWS NET analysts evaluate a given product's departure from a historical mean. This is particularly true for near-real-time products that do not have the benefit of anchoring to station observations. While the IMERG product's spatial resolution, temporal latency, and, for this example, agreement with the CHIRPS shows great promise, its utility for FEWS NET will be better assessed when a longer time series is available.

Disease tracking. TRMM and GPM rainfall estimates have contributed to understanding, monitoring, and predicting vectorborne disease risk. The transmission of vectorborne disease in human populations is the product of complicated, coupled ecological and social processes. Precipitation variability can influence the dynamics of disease risk in a number of ways: heavy rain can lead to floods that alter vector habitats and also interfere with human access to healthcare, droughts can force vectors and reservoir species into closer contact around scarce water sources, and even moderate precipitation variability influences soil moisture conditions and the formation of puddles and ephemeral ponds that can provide breeding sites for disease vectors. The TRMM precipitation record, which offers over 17 years of subdaily multisensor precipitation estimates, has made it possible to quantify these dynamics in regions that lack adequate in situ precipitation measurement networks. Once these relationships are understood, the reliable, consistent, near-real-time character of TRMM (and now GPM) data products makes them well suited for monitoring precipitation-related variability in vector density and disease risk. Since precipitation tends to be a precursor indicator of risk—rainfall influence on insect breeding habitat, for example, leads disease transmission risk by several weeks—GPM near-real-time data availability can inform risk prediction systems that provide health officials with information at decision-relevant lead times. Examples of successful application of satellite precipitation estimates to the study and prediction of disease dynamics include malaria (Midekisa et al. 2012; Lauderdale et al. 2014; Zinszer et al. 2015), schistosomiasis (Xue et al. 2011), Rift Valley Fever (Guilloteau et al. 2014), cholera (Constantin de Magny et al. 2012; Eisenberg et al. 2013; Jutla et al. 2013), and black plague (MacMillan et al. 2012; Moore et al. 2012; Monaghan et al. 2012), among others. In the case of plague in Uganda, multiple satellite precipitation estimates were employed to demonstrate connections between rainfall variability and disease incidence at seasonal and interannual time scales (Fig. 7).

Numerous research groups have recognized the applicability of satellite precipitation to vectorborne disease analysis (Beck et al. 2000; Machault et al. 2011; Tourre et al. 2009). One successful application is work on malaria risk in the western Amazon (Valle et al. 2013; Zaitchik et al. 2014). Researchers are applying TRMM and GPM precipitation estimates to drive a Land Data Assimilation System (LDAS) implemented at 1-km resolution for malaria-prone regions in Peru and Ecuador. An LDAS is a land surface modeling system that merges advanced water and energy balance models with observational data to produce best-available estimates of hydrologic states and fluxes. In this application, the LDAS adds value to TRMM/GPM precipitation estimates by converting integrated rainfall totals into estimates of soil moisture variability (Fig. 8) and associated changes in ponding potential. The LDAS also applies the TRMM (or GPM) data in combination with higher-resolution satellite-derived information on vegetation and other surface properties, so that even the 0.25° TMPA real-time product can drive meaningful simulation of hydrology at much finer resolution.

In the western Amazon, TMPA 3-hourly precipitation estimates enabled skillful prediction of mosquito breeding site density (i.e., number of suitable puddles and ponds), probability of finding mosquito larvae, and probability of finding adult *Anopheles darlingi* mosquitoes—the most important vector for malaria in the region (Pan et al. 2014). Somewhat surprisingly, it was found that the presence of mosquitos decreased under wetter conditions. This appears to be the case for this region because baseline moisture conditions are generally favorable for mosquitoes, and abnormally wet conditions can flush out surface water

habitats that would otherwise function as breeding sites. The TRMM-informed LDAS was also applied to predict actual malaria case counts reported at health posts across a portion of the Peruvian Amazon over an 11-yr period, and both total precipitation and soil moisture anomaly were found to be significant predictors of malaria case count at several weeks' lead time (Feingold et al. 2013). This research system is being converted to an operational warning system serving the entire region.

While the dynamics identified in the western Amazon are useful for monitoring and predicting risk under typical climate variability, GPM might have an equally important role to play in monitoring extreme precipitation events that could lead to subsequent disease outbreaks. An increase in malaria counts in the Peruvian Amazon in 2012, for example, appears to be associated with a prolonged flood in early 2012 (Pan et al. 2014). In this instance, the precipitation influence on malaria risk is almost certainly mediated by the influence that the flood had on infrastructure and the functioning of health care systems. TRMM and GPM multisatellite precipitation monitoring of hydrological extremes has the potential to inform rapid disaster response that could reduce the cascading health impacts that such an event can cause.

COMMUNITY NEEDS AND VIEW FORWARD. The demonstration of value of NASA Earth science data through applications activities has rapidly

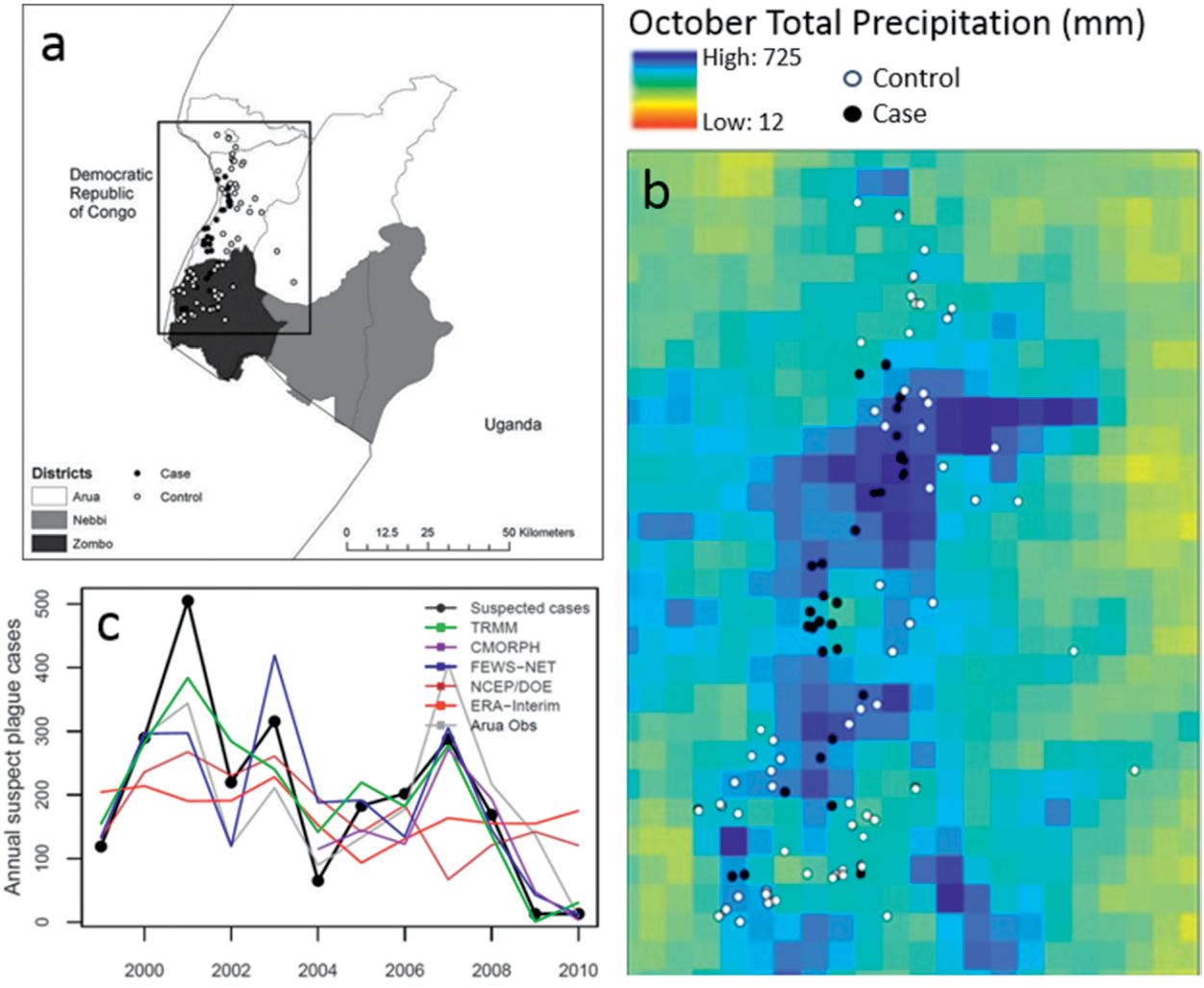

Fig. 7. Rainfall is demonstrated as a valuable predictor of observed plague cases in Uganda, showing (a) distribution of case and control locations in the West Nile region of Uganda (adapted from MacMillan et al. 2012); (b) Oct precipitation totals from 2-km Weather Research and Forecasting Model simulations showing observed and control cases over the boxed area in (a), suggesting cases are associated with wetter, cooler regions (adapted from MacMillan et al. 2012; Monaghan et al. 2012); and (c) predicted number of suspected plague cases by year from modeling that uses different rainfall datasets, including TRMM (adapted from Moore et al. 2012).

become an integral piece in translating satellite data into actionable information and knowledge used to inform policy and enhance decision-making at local to global scales. TRMM and GPM precipitation observations can be quickly and easily accessed via various data portals (see appendix). However, despite significant progress and success in this domain, there remains the challenge of expanding awareness of these data sources across the user community. Feedback on community perspectives and needs was acquired through user workshops held by the GPM Applications team in November 2013 (Ward and Kirschbaum 2014) and June 2015 (Ward et al. 2015), which each had over 125 participants representing government agencies, academia, the private sector, international organizations, and others. Additional feedback has been gained from presentations at scientific meetings, applications-focused workshops, and other events. Three main themes emerged from dialogues and engagement with the applications community: the need for a long and consistent precipitation data record that merges and intercalibrates TRMM with GPM data, the importance of clearly denoted data fields and easy-to-interpret quality-control flags, and the need for easy access and straightforward visualization/export capabilities in a range of different data latencies.

Long data record. One of the major needs articulated by the user and scientific communities is a long, consistent precipitation record. Many of the users applying precipitation data rely on climatologies, anomalies, or distributions based on long-term records to represent extreme precipitation. To be useful for many applications, spatial resolutions finer than 25 km and temporal resolutions less than 3 h are desired, and often required. TMPA barely matches these resolutions, but IMERG is well within these boundaries. There is also a need for an extended precipitation record to consistently calibrate and validate models, metrics, or indicators against past events. The TRMM and GPM algorithm and data processing teams have worked together to reprocess many versions of the Levels 1–3 data when there were significant updates to the code or additional data sources available. In this vein, the GPM team plans to reprocess the IMERG algorithm using GPM and TRMM data and its constellation partners to provide one consistent record of precipitation from 1998 to the present and throughout GPM's lifetime. This work relies on the GPM measurements to improve the database that is used to calibrate all contributing precipitation retrievals. The release of this product is expected in early 2018.

Clear labeling and quality-control fields. The IMERG suite of products has a long list of fields pertinent to the scientific community. These variables include rain rate, which is most relevant for the end-user communities, in addition to random error, probability of liquid precipitation phase, and microwave and IR precipitation fields. The latter provide key

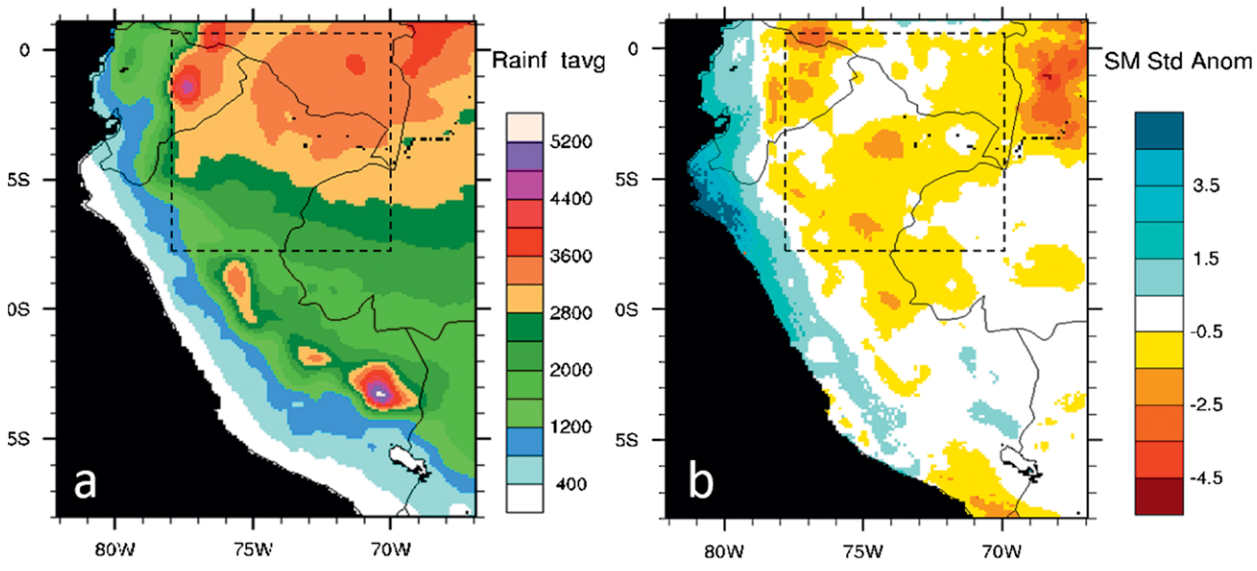

Fig. 8. (a) Long-term mean annual precipitation for Peru and Ecuador based on TMPA data, 1998–2013. (b) Example of a monthly standardized soil moisture anomaly for Mar 1998, when soil moisture anomalies triggered by El Niño rainfall patterns in previous months had left coastal Peru extremely wet and the interior Amazon region anomalously dry. The dashed box shows the approximate location of the western Amazon focus region.

additional information for analysis and validation but can be somewhat confusing to nonexpert users (and sometimes experts as well). Users often have difficulty deciding which product to use, how to understand the error, where to access the data, etc. The GPM team has worked to clarify labeling of the IMERG and other GPM data products to be more accessible to users with different experience levels. One of the recommendations provided by the community was to develop a straightforward quality-control flag that can be used to quickly diagnose the relative quality of the rain and snow data for a particular location and time. The GPM algorithm team is considering developing a qualitative quality flag (e.g., excellent, acceptable, and untrustworthy) ranking to represent the quality of the precipitation data at each spatial and temporal interval.

Data access, latency, and visualization. The user community also specified the need for straightforward data access and visualization capabilities for various experience levels. PPS and the GES DISC have both made great strides to provide user-friendly data formats (GeoTIFF, NetCDF, ASCII) in addition to the native HDF5. There are also new tools in development that will allow more "quick looks" of rain and snow data for rapid assessment to determine if the data product is relevant for a user's specific application. In addition, we have found that the spatial and temporal requirements and type of precipitation data or retrievals needed by different user communities can vary widely. While more expert users are able to ingest the Level 1B brightness temperature or Level 2 precipitation swath data, the majority of the user community is making use of TMPA or IMERG products. Tutorials, training meetings, and webinars have been held to introduce users to GPM data products and solicit feedback on their applications. All training materials are archived and available at http://pmm.nasa.gov/training.

The PPS and GES DISC both allow parameter and spatial subsetting and, for selected products, provide time-averaged variants of these datasets. Data analysis, subsetting, and visualization tools have also been developed to conduct simple data analysis schemes such as time averaging, data comparisons and correlation, and climatology calculations within an online portal such as Giovanni (http://giovanni.gsfc.nasa.gov/giovanni/). There is also a new capability available at https://pmm.nasa.gov/precip-apps to extract IMERG data and other applications products via an Applications Programming Interface (API), where users can directly pull data into their existing systems in a range of different formats and for several different accumulations. Finally, looking forward, there is a growing interest by the community to conduct more sophisticated analyses using online tools to circumvent downloading large volumes of data. There are many programs (e.g., ArcGIS online) that are poised to offer these capabilities; however, there remains a need to more closely link NASA data to these systems.

CONCLUDING REMARKS. TRMM and GPM precipitation data have provided key inputs for a diverse range of user activities to support decision-making for weather forecasting, disasters, agricultural monitoring, and public health, among many others. The successes of TRMM and GPM demonstrate that continuity of precipitation measurements is now a necessity for and expectation of the applications community (Reed et al. 2015). The user community assumes that the precipitation expert community will continue to provide precipitation measurements both continuously and with global homogeneity; however, this is not necessarily the case. NASA is a research agency with a focus on "pioneering" the future in space exploration, scientific discovery, and aeronautics research (www.nasa.gov), and despite the continuity of TRMM to GPM, there is no directed plan for a follow-on mission to GPM. Therefore, it is critical for the user community to provide feedback on data products, quality, and use as well as engage with NASA and other agency precipitation communities, such as NOAA, to help guide the next generation of NASA Earth observation satellites. Outstanding progress has been achieved owing to data sharing among both domestic and international precipitation-focused satellite missions. By continually engaging with the user community, NASA and its partners seek to increase use of GPM precipitation products in a broad range of applications, build capacity to apply Earth science data, and contribute to new satellite mission planning with the goal of promoting new science and applications that benefit society.

ACKNOWLEDGMENTS. This work would not be possible without the contributions of Pete Peterson and Greg Husak (UCSB), NASA's Land Information System team, Jianjun Jin, and the NASA Global Modeling and Assimilation Office. This work was supported by the NASA Precipitation Measurement Missions, NASA Applied Sciences Program Award NNX15AP74G, the FEWS NET's NASA PAPA Water Availability Monitoring Activity, and the NASA Applied Science Disasters Program.

APPENDIX: DATA ACCESS. GPM and TRMM data are available in several different formats. The PMM data access page (https://pmm.nasa.gov/data-access) summarizes all available data. In addition to temporal resolutions shown in Table 2, PPS produces rainfall accumulation for both TMPA and IMERG at 3 h and 1, 3, and 7 days in TIFF format with a worldview file. A subset of the most popular sources for downloading data include the following:

- The PPS Data Products Ordering Interface Science Team Online Request Module (STORM; https://storm.pps.eosdis.nasa.gov/storm/) allows users to search for GPM, partner, and TRMM data; order custom subsets; and set up subscriptions for routine data access. PPS FTP data archives and STORM provide GPM data in HDF5 and GeoTIFF formats.
- The NASA GES DISC (https://daac.gsfc.nasa.gov/) provides an archive of NASA precipitation data obtained from PPS. They have several different ways to access, download, analyze, and graph data. The Giovanni infrastructure (https://giovanni.gsfc.nasa.gov/giovanni/) provides users with an easy-to-use, Web-based interface for the visualization and analysis of global precipitation data. The GES DISC also provides data access through Mirador (https://mirador.gsfc.nasa.gov/), which distributes all files online in multiple formats including HDF5 and NetCDF.
- The PMM web page (https://pmm.nasa.gov/) provides a summary of the data sources and types and has a visualization interface for quick looks at GPM data and related applications, including flood and landslide modeling. From this portal (https://pmm.nasa.gov/precip-apps), a user is able to view the last 60 days of data from the IMERG products (Early, Late) as well as export subsets of this data via a range of different formats including GeoTIFF, PNG, and access the data via Application Programming Interface (API).

REFERENCES

AGRHYMET, 1996: Méthodologie de suivi des zones à risque. AGRHYMET FLASH, Bulletin de Suivi de la Campagne Agricole au Sahel 0/96, Vol. 2, 2 pp. [Available from Centre Regional AGRHYMET, B.P. 11011, Niamey, Niger.]

Beck, L. R., B. M. Lobitz, and B. L. Wood, 2000: Remote sensing and human health: New sensors and new opportunities. *Emerging Infect. Dis.*, **6**, 217–227, doi:10.3201/eid0603.000301.

Brown, M. E., and K. M. de Beurs, 2008: Evaluation of multi-sensor semi-arid crop season parameters based on NDVI and rainfall. *Remote Sens. Environ.*, **112**, 2261–2271, doi:10.1016/j.rse.2007.10.008.

——, and V. M. Escobar, 2014: Assessment of soil moisture data requirements by the potential SMAP data user community: Review of SMAP mission user community. *IEEE J. Sel. Top. Appl. Earth Obs. Remote Sens.*, **7**, 277–283, doi:10.1109/JSTARS.2013.2261473.

Constantin de Magny, G., and Coauthors, 2012: Cholera outbreak in Senegal in 2005: Was climate a factor? *PLoS One*, **7**, e44577, doi:10.1371/journal.pone.0044577.

Eisenberg, M. C., G. Kujbida, A. R. Tuite, D. N. Fisman, and J. H. Tien, 2013: Examining rainfall and cholera dynamics in Haiti using statistical and dynamic modeling approaches. *Epidemics*, **5**, 197–207, doi:10.1016/j.epidem.2013.09.004.

Feingold, B. J., B. F. Zaitchik, A. Sandoval, C. A. Antonio, R. P. Z. Vasquez, and W. K. Pan, 2013: Climate and land use drivers of the spatial and temporal distribution of malaria risk in the Peruvian Amazon. *Proc. Conf. on Environment and Health*, Basel, Switzerland, International Society for Environmental Epidemiology, Abstract 4668. [Available online at http://ehp.niehs.nih.gov/isee/p-3-12-07/.]

FEWS-NET, 2016: Joint EC, FAO, FEWS NET and WFP statement on El Niño impact in southern Africa. Famine Early Warning Systems Network, accessed 3 May 2016. [Available online at www.fews.net/southern-africa/alert/february-2016.]

Funk, C., and Coauthors, 2015: The climate hazards infrared precipitation with stations—A new environmental record for monitoring extremes. *Sci. Data*, **2**, 150066, doi:10.1038/sdata.2015.66.

Gray, E., 2015: Satellite-based flood monitoring central to relief agencies' disaster response. NASA, accessed 3 May 2016. [Available online at www.nasa.gov/feature/goddard/satellite-based-flood-monitoring-central-to-relief-agencies-disaster-response.]

Guha-Sapir, D., R. Below, and P. Hoyois, 2014: EM-DAT: The CRED/OFDA International Disaster Database. Université Catholique de Louvain, accessed 20 March 2014. [Available online at www.emdat.be/database.]

Guilloteau, C., M. Gosset, C. Vignolles, M. Alcoba, Y. M. Tourre, and J.-P. Lacaux, 2014: Impacts of satellite-based rainfall products on predicting spatial patterns of rift valley fever vectors. *J. Hydrometeor.*, **15**, 1624–1635, doi:10.1175/JHM-D-13-0134.1.

Hong, Y., K. L. Hsu, X. G. Gao, S. Sorooshian, and X. Gao, 2004: Precipitation Estimation from Remotely

Sensed Imagery using an Artificial Neural Network Cloud Classification System. *J. Appl. Meteor.*, **43**, 1834–1852, doi:10.1175/JAM2173.1.

Hou, A. Y., and Coauthors, 2014: The Global Precipitation Measurement Mission. *Bull. Amer. Meteor. Soc.*, **95**, 701–722, doi:10.1175/BAMS-D-13-00164.1.

Huffman, G. J., and Coauthors, 2007: The TRMM Multisatellite Precipitation Analysis (TMPA): Quasi-global, multiyear, combined-sensor precipitation estimates at fine scales. *J. Hydrometeor.*, **8**, 38–55, doi:10.1175/JHM560.1.

——, R. F. Adler, D. T. Bolvin, and E. J. Nelkin, 2010: The TRMM Multi-satellite Precipitation Analysis (TMPA). *Satellite Rainfall Applications for Surface Hydrology*, F. Hossain and M. Gebremichael, Eds., Springer, 3–22.

——, D. T. Bolvin, D. Braithwaite, K. Hsu, R. J. Joyce, C. Kidd, E. J. Nelkin, and P. Xie, 2015: NASA Global Precipitation Measurement Integrated Multi-satellitE Retrievals for GPM (IMERG). Algorithm Theoretical Basis Doc., version 4.5, 30 pp. [Available online at http://pmm.nasa.gov/sites/default/files/document_files/IMERG_ATBD_V4.5.pdf.]

Jayanthi, H., G. J. Husak, C. Funk, T. Magadzire, A. Adoum, and J. P. Verdin, 2014: A probabilistic approach to assess agricultural drought risk to maize in Southern Africa and millet in Western Sahel using satellite estimated rainfall. *Int. J. Disaster Risk Reduct.*, **10**, 490–502, doi:10.1016/j.ijdrr.2014.04.002.

Joyce, R. J., and P. Xie, 2011: Kalman filter–based CMORPH. *J. Hydrometeor.*, **12**, 1547–1563, doi:10.1175/JHM-D-11-022.1.

Jutla, A., and Coauthors, 2013: Environmental factors influencing epidemic cholera. *Amer. J. Trop. Med. Hyg.*, **89**, 597–607, doi:10.4269/ajtmh.12-0721.

Kidd, C., A. Becker, G. Huffman, C. Muller, P. Joe, G. Skofronick-Jackson, and D. Kirschbaum, 2017: So, how much of the Earth's surface is covered by rain gauges? *Bull. Amer. Meteor. Soc.*, **98**, 69–78, doi:10.1175/BAMS-D-14-00283.1.

Kucera, P. A., E. E. Ebert, J. F. Turk, V. Levizzani, D. Kirschbaum, F. J. Tapiador, A. Loew, and M. Borsche, 2013: Precipitation from space: Advancing Earth system science. *Bull. Amer. Meteor. Soc.*, **94**, 365–375, doi:10.1175/BAMS-D-11-00171.1.

Kummerow, C., W. Barnes, T. Kozu, J. Shiue, and J. Simpson, 1998: The Tropical Rainfall Measuring Mission (TRMM) sensor package. *J. Atmos. Oceanic Technol.*, **15**, 809–817, doi:10.1175/1520-0426(1998)015<0809:TTRMMT>2.0.CO;2.

Lauderdale, J. M., and Coauthors, 2014: Towards seasonal forecasting of malaria in India. *Malar. J.*, **13**, 310, doi:10.1186/1475-2875-13-310.

Liang, X., D. P. Lettenmaier, E. F. Wood, and S. J. Burges, 1994: A simple hydrologically based model of land surface water and energy fluxes for general circulation models. *J. Geophys. Res.*, **99**, 14 415–14 428, doi:10.1029/94JD00483.

Machault, V., C. Vignolles, F. Borchi, P. Vounatsou, F. Pages, S. Briolant, J.-P. Lacaux, and C. Rogier, 2011: The use of remotely sensed environmental data in the study of malaria. *Geospat. Health*, **5**, 151–168, doi:10.4081/gh.2011.167.

MacMillan, K., and Coauthors, 2012: Climate predictors of the spatial distribution of human plague cases in the West Nile region of Uganda. *Amer. J. Trop. Med. Hyg.*, **86**, 514–523, doi:10.4269/ajtmh.2012.11-0569.

Midekisa, A., G. Senay, G. M. Henebry, P. Semuniguse, and M. C. Wimberly, 2012: Remote sensing-based time series models for malaria early warning in the highlands of Ethiopia. *Malar. J.*, **11**, 165, doi:10.1186/1475-2875-11-165.

Molod, A., L. Takacs, M. Suarez, and J. Bacmeister, 2015: Development of the GEOS-5 atmospheric general circulation model: Evolution from MERRA to MERRA2. *Geosci. Model Dev.*, **8**, 1339–1356, doi:10.5194/gmd-8-1339-2015.

Monaghan, A. J., K. MacMillan, S. M. Moore, P. S. Mead, M. H. Hayden, and R. J. Eisen, 2012: A regional climatography of West Nile, Uganda, to support human plague modeling. *J. Appl. Meteor. Climatol.*, **51**, 1201–1221, doi:10.1175/JAMC-D-11-0195.1.

Moore, S. M., A. Monaghan, K. S. Griffith, T. Apangu, P. S. Mead, and R. J. Eisen, 2012: Improvement of disease prediction and modeling through the use of meteorological ensembles: Human plague in Uganda. *PLoS One*, **7**, e44431, doi:10.1371/journal.pone.0044431.

NASA, 2015: NASA Global Precipitation Measurement (GPM) level 1C algorithms. Algorithm Theoretical Basis Doc., 48 pp. [Available online at http://pps.gsfc.nasa.gov/Documents/L1C_ATBD.pdf.]

Pan, W., O. Branch, and B. Zaitchik, 2014: Impact of climate change on vector-borne disease in the Amazon. *Global Climate Change and Public Health*, E. K. Pinkerton and N. W. Rom, Eds., Springer, 193–210, doi:10.1007/978-1-4614-8417-2_11.

Reed, P. M., N. W. Chaney, J. D. Herman, M. P. Ferringer, and E. W. Wood, 2015: Internationally coordinated multi-mission planning is now critical to sustain the space-based rainfall observations needed for managing floods globally. *Environ. Res. Lett.*, **10**, 024010, doi:10.1088/1748-9326/10/2/024010.

Senay, G. B., and J. Verdin, 2003: Characterization of yield reduction in Ethiopia using a GIS-based crop

water balance model. *Can. J. Rem. Sens.*, **29**, 687–692, doi:10.5589/m03-039.

Shepherd, J. M., S. Burian, C. Liu, and S. Bernardes, 2016: Satellite precipitation metrics to study the energy-water-food nexus within the backdrop of an urbanized globe. Earthzine, accessed 3 May 2016. [Available online at http://earthzine.org/2016/05/31/satellite-precipitation-metrics-to-study-the-energy-water-food-nexus-within-the-backdrop-of-an-urbanized-globe/.]

Simpson, J., C. Kummerow, W.-K. Tao, and R. F. Adler, 1996: On the Tropical Rainfall Measuring Mission (TRMM). *Meteor. Atmos. Phys.*, **60**, 19–36, doi:10.1007/BF01029783.

Stewart, S., 2014: Hurricane Julio Discussion Number 10. National Hurricane Center, accessed 3 May 2016. [Available online at www.nhc.noaa.gov/archive/2014/ep10/ep102014.discus.010.shtml.]

——, and C. Jacobson, 2016: Hurricane Julio. NHC Tropical Cyclone Rep. 18 pp. [Available online at www.nhc.noaa.gov/data/tcr/EP102014_Julio.pdf.]

Tourre, Y. M., J.-P. Lacaux, C. Vignolles, and M. Lafaye, 2009: Climate impacts on environmental risks evaluated from space: A conceptual approach to the case of Rift Valley Fever in Senegal. *Global Health Action*, **2**, 2053, doi:10.3402/gha.v2i0.2053.

USGS, 2016: How much water is there on, in, and above the Earth? USGS Water Science School, accessed 6 May 2016. [Available online at http://water.usgs.gov/edu/earthhowmuch.html.]

Valle, D., B. Zaitchik, B. Feingold, K. Spangler, and W. Pan, 2013: Abundance of water bodies is critical to guide mosquito larval control interventions and predict risk of mosquito-borne diseases. *Parasites Vectors*, **6**, 179, doi:10.1186/1756-3305-6-179.

Verdin, J., and R. Klaver, 2002: Grid-cell-based crop water accounting for the famine early warning system. *Hydrol. Processes*, **16**, 1617–1630, doi:10.1002/hyp.1025.

Wang, X., D. Parrish, D. Kleist, and J. Whitaker, 2013: GSI 3DVar-based ensemble–variational hybrid data assimilation for NCEP Global Forecast System: Single-resolution experiments. *Mon. Wea. Rev.*, **141**, 4098–4117, doi:10.1175/MWR-D-12-00141.1.

Ward, A., and D. Kirschbaum, 2014: Measuring rain for society's gain: A GPM Applications Workshop. *The Earth Observer*, Vol. 26, Issue 1, NASA Goddard Space Flight Center, Greenbelt, MD, 26–34. [Available online at http://eospso.nasa.gov/sites/default/files/eo_pdfs/Jan-Feb_2014_final_color_508.pdf.]

——, D. Kirschbaum, and M. Hobish, 2015: Measuring rain and snow for science and society: The Second GPM Applications Workshop. *The Earth Observer*, Vol. 27, Issue 5, NASA Goddard Space Flight Center, Greenbelt, MD, 4–11. [Available online at http://eospso.nasa.gov/sites/default/files/eo_pdfs/Sep_Oct_2015_color_508.pdf#page=4.]

WMO, 1992: *International Meteorological Vocabulary.* World Meteorological Organization, 784 pp.

Wu, H., R. F. Adler, Y. Hong, Y. Tian, and F. Policelli, 2012: Evaluation of global flood detection using satellite-based rainfall and a hydrologic model. *J. Hydrometeor.*, **13**, 1268–1284, doi:10.1175/JHM-D-11-087.1.

——, ——, Y. Tian, G. J. Huffman, H. Li, and J. Wang, 2014: Real-time global flood estimation using satellite-based precipitation and a coupled land surface and routing model. *Water Resour. Res.*, **50**, 2693–2717, doi:10.1002/2013WR014710.

Xue, Z., M. Gebremichael, R. Ahmad, M. L. Weldu, and A. C. Bagtzoglou, 2011: Impact of temperature and precipitation on propagation of intestinal schistosomiasis in an irrigated region in Ethiopia: Suitability of satellite datasets. *Trop. Med. Int. Health*, **16**, 1104–1111, doi:10.1111/j.1365-3156.2011.02820.x.

Zaitchik, B. F., B. Feingold, D. Valle, and W. Pan, 2014: Integrating earth observations to support malaria risk monitoring in the Amazon. Earthzine, accessed 3 May 2016. [Available online at www.earthzine.org/ 2014/04/14/integrating-earth-observations-to-support-malaria-risk-monitoring-in-the-amazon/.]

Zinszer, K., R. Kigozi, K. Charland, G. Dorsey, T. F. Brewer, J. S. Brownstein, M. R. Kamya, and D. L. Buckeridge, 2015: Forecasting malaria in a highly endemic country using environmental and clinical predictors. *Malar. J.*, **14**, 245, doi:10.1186/s12936-015-0758-4.